On-sun Testing of Miscibility Gap Alloy Thermal Storage

Mark Copus[1], Benjamin Fraser[1], Roger Reece[2], Stuart Hands[2], Dylan Cuskelly[1], Heber Sugo[1], Samuel Reed[1], James Bradley[1], Alexander Post[1] and Erich Kisi[1†]

[1] *School of Engineering, The University of Newcastle, Callaghan NSW 2308, Australia*

[2] *CSIRO Energy Centre, Mayfield West NSW 2304, Australia*

Abstract

The ability of a C-Zn Miscibility Gap Alloy (MGA) material to operate as a combined solar receiver and storage was investigated. MGA thermal energy storage materials comprise metallic PCM particles embedded within a conducting metal or semi-metal matrix to form a macroscopically solid combined latent heat/sensible heat storage material. A receiver containing 4 x 1L MGA storage modules was mounted on a solar concentrating dish. The storage material was directly illuminated by concentrated solar radiation at a flux of approximately 105 kW/m^2, readily attaining surface temperatures of 520-530 °C, well above the phase change temperature of 420 °C. Single step charging led to a state of charge of 80 % without exceeding a nominal surface temperature of 530 °C. Cycling on and off sun in the range 460 – 520 °C was used to achieve a state of 99 % charged. Thermal performance of the MGA during solar charging and its discharge by natural cooling is presented and analysed.

Keywords: Thermal storage, Phase change material, Concentrated solar power, Solar absorption

1. Introduction

Thermal energy and its management is a crucial part of the Concentrated Solar thermal Power (CSP) industry. As a consequence, thermal energy storage (TES) technologies, to overcome solar intermittency and to allow electricity generation into the evening, have been under development for several decades. At the heart of each TES technology is a thermal storage material. A wide variety of potential TES materials have been studied, falling into the broad storage categories of solid sensible heat, liquid sensible heat and phase change materials (PCM). The relative merits of the respective classes of material and the properties of individual materials have been the subject of a number of exhaustive reviews (Kenisarin, 2010, Laing et al., 2012, Rathod et al., 2013, Tian et al., 2013, Kuravi et al., 2013, Khan et al., 2016, Alva, et al., 2017, Dutta, 2017, Pelay et al., 2017, Xu et al., 2015). In general, it may be concluded that most of the PCM studied, although theoretically more energy dense, suffer from a number of limitations in regards to application for CSP. Primarily, this is the low thermal conductivity of all but the metallic systems. Significant reduction in energy density and increase in complexity and cost is incurred by the necessary heat transfer enhancements (Agyenim et al., 2010, Liu et al., 2012, Gomez, 2011) which are generally only partially successful. Metallic PCM on the other hand, generally have containment problems and associated safety issues (Fukahori et al., 2016). Consequently, operational CSP plants with TES installed use sensible heat storage materials.

† Corresponding Author
E-mail: erich.kisi@newcastle.edu.au

To be successful, a TES material needs to be coupled with the appropriate infrastructure to make a working TES technology. At present, the industry standard TES technology is two-tank sensible heat storage based on molten nitrate salts (Herrmann et al. 2004, Dutta, 2017, Gonzalez-Roubaud et al.,

2017, Kuravi et al., 2013). These salts, which are generally a eutectic mixture of $NaNO_3$ and KNO_3, sometimes modified by additives to adjust the maximum and minimum allowable temperatures, are the principal storage material in parabolic trough CSP plants worldwide ("Parabolic Trough Projects", 2018) as well as having been adapted to solar power tower plants in a number of locations ("Power Tower Projects", 2018). Although the exact layout and mode of operation can vary from the use of thermoclines to vigorously pumped forced convection, there are three major features that molten salt TES technologies have in common. First, there is significant plant complexity, generally involving separate receiver, storage and steam generation systems connected by multiple heat exchangers. Second, there is a significant parasitic energy cost of maintaining the salt in a molten state throughout the entire system[1]. Third, the energy density is dictated by an operational range between the melting temperature of the salt (T_{min}) and its decomposition temperature (T_{max}). Although molten salt technologies have been successfully implemented at numerous sites, there is a continuing strong demand for cost reduction in CSP with storage, as it has been argued this has the best chance of providing on-demand large scale solar generated electricity in the foreseeable future (CSP – Technology Brief, 2013).

A new type of TES technology, based on Miscibility Gap Alloys (MGA) was proposed with the three-fold aim of eliminating parasitic energy losses, increasing energy density and decreasing plant complexity (Sugo et al. 2013, Reed et al. 2018). Considering these in turn, MGA materials are macroscopically solid at all temperatures accessible under normal operation. However, they contain a high volume fraction (typically 50 vol%) of dispersed metal particles with a lower melting temperature (T_m) which acts as a PCM embedded within the solid metal or semi-metal matrix. The microstructure is carefully controlled during manufacture so that the PCM particles do not meet the percolation threshold at which there could be leakage of the PCM above its melting temperature. Instead, with the properly engineered microstructure, the PCM is safely encapsulated in a high thermal conductivity matrix; melting and freezing as needed, without parasitic energy cost.

Thermal energy is stored within MGA as a combination of the latent heat of melting of the PCM particles and the considerable sensible heat of both the matrix and the PCM material. MGA can therefore provide significant stored energy density close to a temperature that is technically interesting due to the operating point of turbomachinery or other energy conversion technology, or the delivery temperature of an energy capture process. Because of this, MGA energy density is usually quoted within the band $T_m \pm 50°C$ with values in the range 0.5 – 1.1 MJ/L routinely accessible (Reed et al. 2018). If the entire thermal energy content is considered above a 'useful' cut-off, say 200 °C, substantially more energy is available (0.8 – 2.1 MJ/L).

The plant complexity associated with installed molten salt storage plants is broadly associated with heat exchange and the two-tank liquid storage system (Herrmann et al., 2004, Tyner et al., 1995, Ramorakane et al., 2016). Sunlight is converted into heat at the solar receiver which is cooled by a heat transfer fluid (HTF). Taking conventional trough plants as an example, the HTF is often a thermal-oil or a gas. This HTF is transported to a heat exchanger where it heats the already molten salt[2] to the storage temperature

[1] Typically 10-15% in summer months and up to 24% in winter depending upon location (Tyner et al., 1995, Kolb et al., 2002, Ramorakane et al., 2016).
[2] i.e. there is no role for latent heat here.

whereupon it is pumped into the hot tank. When required, the heated molten salt is pumped from the hot tank via a heat exchanger where water is boiled and the steam superheated ready for expansion through a turbine. The cooled salt is stored in a cold tank ready to be heated again in the next cycle. Simplifications in the form of heating the molten salt directly at the receiver and the use of a thermocline system rather than pumping can reduce this complexity however reliance on rapidly moving fluids and counter-current fluid-fluid heat exchangers remains. The durability and compatibility of solar receiver materials at high concentration ratios is also of great concern (Sarvghad et al., 2018).

MGA storage materials, being macroscopically solid with high thermal conductivity, offer different challenges and opportunities. The simplest implementation of MGA storage is to assemble smaller MGA modules into a large solid storage block. This macroscopically solid storage block, suitably insulated, can simultaneously function as the solar receiver, the thermal energy storage and the boiler (or heat exchanger) all in one. Such a configuration has substantially lower infrastructure requirement and therefore exhibits substantially lower projected installation and maintenance costs.

In order to bring this ideal situation into practical realisation in CSP or other long term thermal energy storage applications, MGA materials require scaled up testing. The first key requirement is a demonstration of scaled up storage capacity from laboratory scale (0.05 – 0.2 L), to storage blocks of several litres. A second requirement is to demonstrate unrestricted heat transfer within a storage block built up from smaller MGA modules. An important third requirement is to prove the ability to survive direct irradiation in a solar receiver. This work reports the first results for on-sun testing of a 4-module MGA storage block using a parabolic dish concentrator within which each of these requirements are shown to be met in the short term and under the conditions of the test.

2. Experimental

The system chosen for study uses Zn as the PCM and graphite as the matrix phase. In this system, latent heat is stored and delivered close to the melting temperature of Zn, 420 °C. Four MGA thermal energy storage modules were manufactured using pure graphite (AMPS - Australian Metal Powder Supplies, 45μm) and Zn particles (AMPS, ”Coarse Powder”, 1.5 ±0.5 mm) according to a procedure previously described (Copus et al. 2017). Graphite powder was mixed with a surplus of a 37.5% sodium silicate solution in water to act as a binder. Excess binder solution was allowed to drain out of the mixture followed by drying in an air oven at 90 °C. The graphite was then broken up again by grinding followed by mixing with the Zn particles at 50 % by volume. The mixed powder was pressed in a square 140 x 140 mm die to a green height of 50 mm. The pressed modules were wrapped in Al foil to exclude air and fired at 500 °C for 8 h in air using a 5 °C/min heating ramp. Apart from minimal leakage of molten Zn from a few particles in direct contact with the surface, the Zn remained encapsulated as previously reported (Sugo et al. 2013). Four control modules were sawn from commercial graphite (“Grade PFR”, GES, 1.72g/cm^3,) to be 140 x 140 x 50 mm in size. The theoretical properties of a stack of four MGA modules (totalling 3.87 L) and a stack of four graphite control modules (3.92 L in total), are summarised in Table 1.

Table 1 – Properties and theoretical stored energy of four MGA and graphite modules

Material	Thermal conductivity (W/mK)*	Thermal diffusivity (m^2/s)	Energy stored for $T_m \pm 50$ °C (MJ) [3]	Energy stored 200 °C – T_m + 50 °C (MJ) [3]	Measured Density (kg/L)
C	160	6.156×10^{-5}	1.02	2.53	1.72
C-Zn	83-86	1.548×10^{-5}	2.41	4.01	3.99

* *At room temperature*

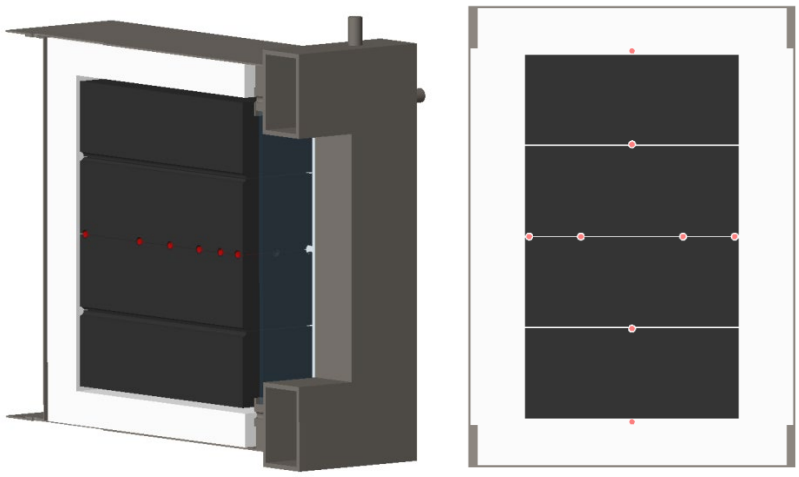

Figure 1 – CAD model of the solar receiver and storage block: a) centreline longitudinal section and b) transverse section 10mm inside the illuminated face. Thermocouple positions are shown by red dots.

An insulated solar receiver was constructed to house a storage block comprising the four storage modules as illustrated in Figure 1. In all description or discussion of the receiver, the window end will be referred to as the front and the opposite end as the back regardless of the orientation of the receiver during solar illumination. The receiver was assembled by placing a stack of four storage modules (black) within an outer stainless steel shell (grey) lined with 50 mm thick insulation shown in white (Superwool Plus Board 85, Morgan Thermal Ceramics). The front face incorporated a high transmissivity heat resisting glass window mounted 50 mm in front of the storage modules. A steel water channel, 50 mm deep, was situated in front of the window in case cooling of the glass was required. The cooling channel and exterior of the receiver was protected from direct irradiation by a stainless steel shield with a 200 mm x 120 mm aperture. As shown by the red dots in Figure 1, fourteen thermocouples were installed into 20 mm deep holes and exited at the rear of the receiver along thin slots cut into the modules. Six primary thermocouples measured the temperature along the centre axis of the storage block, between the second and third module at 5, 15, 25, 45, 80 and 135 mm from the illuminated face of the C-Zn modules for thermocouples 1-6 respectively. The remaining thermocouples were distributed 10 mm behind the front face, equally spaced parallel and perpendicular to the stack. Thermocouple signals were sampled at 1 Hz, then averaged and recorded for each 10 s interval.

The receiver was mounted on a parabolic dish concentrator at the CSIRO Energy Centre as shown in Figure 2. The dish has a daisy configuration with mirrors arranged in 5 major petals. At this site, the DNI is typically in the range 900-1050 W/m^2 in the early afternoon during summer when the experiments were conducted. After initial feasibility checks using just one of the five petals of mirrors installed, all subsequent tests used two petals of mirrors. The dish in this state, can deliver ~6 kW of concentrated sunlight over a central spot ~270 mm in diameter with average flux approximately 105

[3] Stored energy here has been corrected for the actual graphite density which is lower than the theoretical value.

kW/m^2 with unknown energy distribution. The opening in the receiver and window is just 200 mm x 120 mm allowing at most 42% by area of the central spot to enter the receiver. However, as the storage block was set back 113 mm from the outer stainless steel aperture, there was also considerable unavoidable shadowing of the storage material from the incident light by the walls of the cavity.

Figure 2 – The receiver/storage unit (arrowed) mounted on the parabolic dish.

As the storage modules were prepared at 500 °C, it was considered prudent to set an upper limit of 530 °C for these initial on-sun tests although it is expected that they can tolerate much higher temperatures. In particular, graphite is routinely used in high temperature equipment, in air below 450 °C and in furnaces at more than 2000 °C provided a vacuum or reducing environment is present. Since the oxidation of graphite at the temperature s of this test produces CO, a highly reducing gas, it is sufficient to seal the receiver box to prevent continuing oxidation.

The experiments commenced using the control graphite storage block. On-sun testing was conducted by driving the concentrator into the collecting position and tracking until the front thermocouple (TC1) registered 520 °C. Thereafter, the dish was turned off-sun and the thermocouples were monitored for a further 40 minutes.

Having successfully demonstrated the apparatus and methodology, the receiver was re-loaded with the four C-Zn MGA modules and returned to the dish concentrator several weeks later. The dish was driven into position and the sun tracked until the front thermocouple registered 531 °C (> our nominal maximum temperature). At the end of this test, the rearmost thermocouple, 5 mm from the rear of the storage block, registered 417 °C, just below the melting point of Zn (420 °C) i.e. the modules were not quite fully charged with thermal energy. The dish was taken off-sun and the thermocouples monitored for a further 19.5 h by which time the storage block had cooled to 45 °C.

In order to fully charge the modules without exceeding the nominal maximum temperature, a second MGA run was conducted in which the receiver was heated on-sun until the front thermocouple registered 509 °C followed by oscillating in and out of the concentrating position thirteen times over a 33 minute period so that the temperature of the front thermocouple remained within a band approximately 470 – 510 °C. This allowed the rearmost thermocouple to attain a temperature of 448

°C, well above the melting point of Zn. In this condition, the MGA storage should have been fully charged.

3. Results

3.1 Temperature response and distribution

The temperature distribution as a function of time along the centreline of the 4-module graphite control block is shown in colour at the left of Figure 3. It may be seen that the graphite storage block is able to easily tolerate direct irradiation and has adequate conductivity to redistribute the heat rapidly. When the foremost thermocouple is at its maximum temperature, the temperature difference from the front to the back of the block is only 44 °C (across 130mm). Thermocouples TC9 – TC14 situated laterally, above and below the centreline (see Figure 1) did not differ by more than 6°C. When the receiver was moved off-sun, the graphite block appeared to cool extremely rapidly initially. This is the result of internal redistribution of heat by conduction and does not reflect true heat loss i.e. between approximately 3700 and 3800 seconds, the front face was observed to cool while the back of the block continued to increase in temperature. After just 2 minutes off-sun, the temperature difference in thermocouples 1-6 was less than 2 °C. Thereafter, the remaining temperature change is primarily heat loss by a combination of re-radiation through the glass receiver window and the combined effect of conduction through the receiver wall and convection to the outside atmosphere. As graphite stores only sensible heat, the temperature continuously decays to ambient (shown dashed below 408 °C).

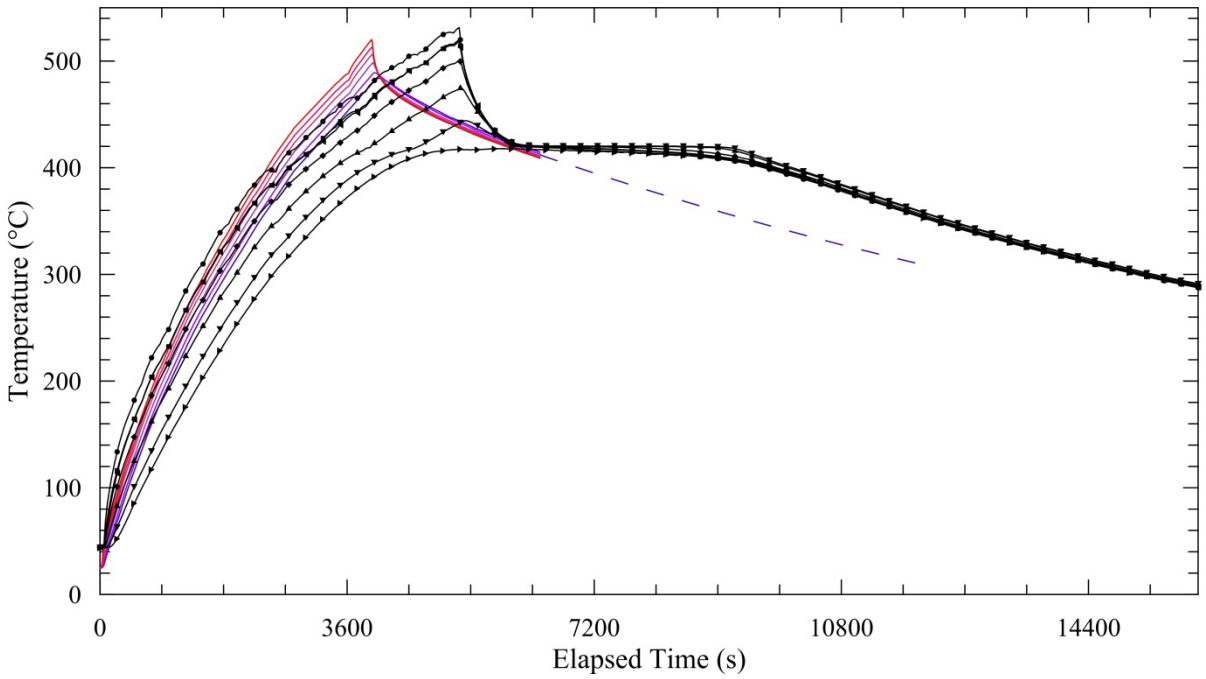

Figure 3 – (Colour online) Temperature profiles from the C-Zn MGA 4-module storage block (● - TC1, ■ - TC2, ◆ - TC3, ▲ - TC4, ▼ - TC5 and ► - TC6) during the first run of on-sun heating by direct irradiation and a portion of the off-sun cooling period in ambient air. Only every 25th data point is shown. Also shown are profiles from the control graphite storage block transitioning from TC1 (red) at the absorption side to TC6 (blue) at the rear of the receiver and subsequent extrapolated cooling curve

The major portion of Figure 3, shown in black, is dedicated to the first run using the 4-module C-Zn MGA storage block. On heating, the temperature rise is initially comparable to the graphite at the

receiver face (TC1). However, the rate of heat flow is reduced by the lower thermal conductivity (Table 1) and decreased thermal diffusivity due to the presence of Zn (i.e. greater thermal mass; Table 1). Minimal thermal arrest at the phase change temperature (420 °C) is observed in thermocouples near the front face of the receiver (TC1-TC3) as the thermocouples are small (1.6 mm ϕ) and the phase change front is moving rapidly. Small thermal arrests are visible for TC4 and TC5 whereas TC6 stagnated at 417 °C, never attaining the phase change temperature.

When the receiver was moved off-sun, there was a sharp drop in the temperature at the front of the storage block, similar to, but slower than that for the graphite. This was followed by a pronounced thermal arrest at all positions for approximately 2800 s (0.78 h) giving a very uniform discharge of energy throughout the block during the phase transition and indeed thereafter during free cooling. This temperature decay will later be used to estimate stored energy and incident flux (§ 3.2).

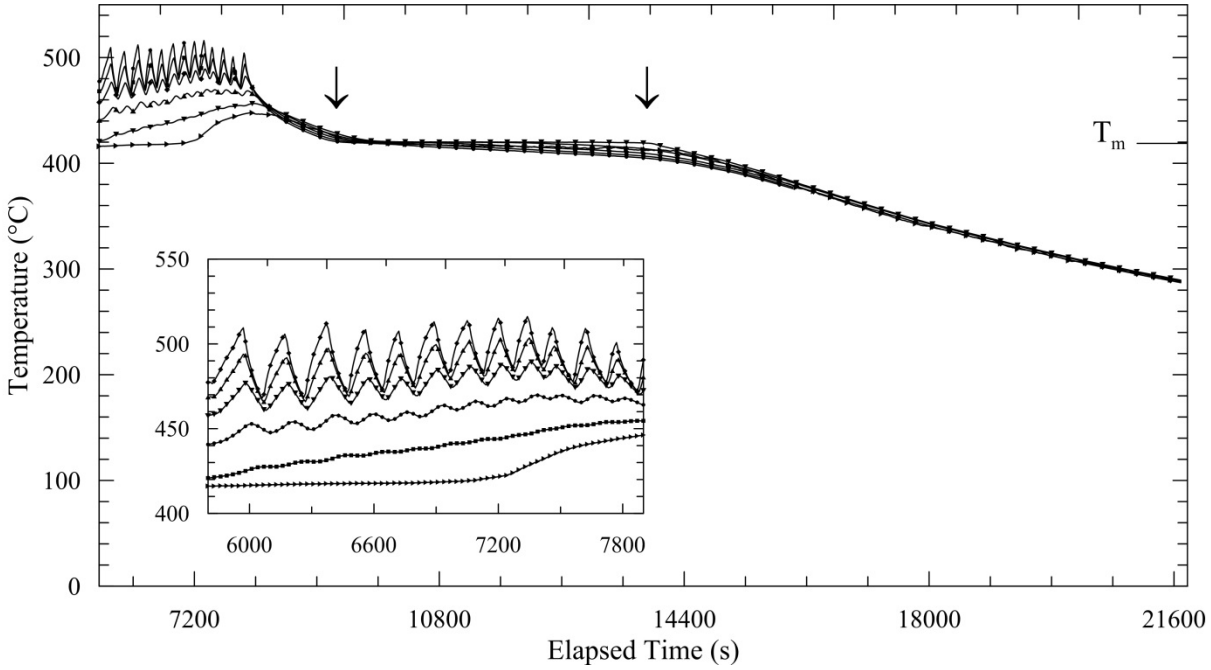

Figure 4 – Temperature profiles from the C-Zn MGA 4-module storage block (● - TC1, ■ - TC2, ◆ - TC3, ▲ - TC4, ▼ - TC5 and ► - TC6) during oscillation on-off sun followed by off-sun cooling in ambient air. The inset shows damping of the temperature fluctuations deeper within the storage block on axes with the same units. The phase change temperature T_m is shown as well as arrows marking the approximate beginning and end of the phase change.

Figure 4 presents temperature data recorded from the 4-module C-Zn block during and after on-off sun oscillation to facilitate complete thermal loading. The temperature profile of the rearmost thermocouple, TC6, reaches the phase change temperature outside the left hand edge of the graph and remains at near-constant temperature for the next 20 minutes, to an 'elapsed time' of approximately 7200 s, before rising slowly to 448 °C. From this behaviour and by considering the thermocouple position, just 5 mm from the rear of the storage block on the centreline, it is safe to assume that the storage block was fully charged when the receiver was re-positioned off-sun at the end of the loading part of the test. Consequently, in this test, the thermal arrest visible in Figure 4 is much more pronounced than in the

first test (Figure 3), lasting for approximately 4500 s (1.25 h). As with the other tests, the cooling data represent the total system heat losses and will be further analysed in §3.2.

3.2 Heat flow analysis

The measured temperatures at each time step were used to obtain an estimate for the heat flow in and out of the storage block. Through this analysis, the power absorbed at the front face of the storage block, the net power retained within the storage block and the fraction of the latent heat accessed during each charging event was calculated.

For convenience, Table 2 defines the different heat flow terms used in this section.

Table 2 – Definitions of heat flow analysis terms

Term	Meaning	Origin
q_{net}	Net power absorbed into the storage block	Measured
q_{abs}	Power absorbed from the incident flux at the front face of the storage block	Derived
q_{out}	Rate of heat loss from the storage module	Measured
q^*_{out}	Approximate rate of heat loss	Modelled

The *net* power absorbed by the block, q_{net}, is the difference between the power absorbed from the incident radiation, q_{abs}, and the system losses, q_{out}:

$$q_{net} = q_{abs} - q_{out} \quad (1)$$

and can be directly calculated from the experimental data during absorption using:

$$q_{net(T)} = mC_{p(T)}\frac{dT}{dt} \quad (2)$$

where m is the mass of storage material and $C_{p(T)}$ its specific heat capacity at temperature T.

In the current work, no controlled heat extraction was installed within the storage block, nor was an insulated shutter available. Because of this, when off-sun, the receiver was cooled by natural heat losses only. The rate of heat loss from the storage medium as a function of temperature during cooling *below the phase change* is given by:

$$q_{out(T)} = mC_{p(T)}\frac{dT}{dt} \quad (3)$$

Application of eqn. (3) to the temperature data from the 4-module C-Zn storage block over the range below the phase change to the right of Figure 3, where only sensible heat is being lost, was used to calculate $q_{out(T)}$. However, the losses during the heating and phase change sections are also of interest, as such, a model for the entire temperature range was derived using the experimentally determined q_{out}.

Thermal losses from the receiver are due to thermal radiation combined with conduction to and convection from all of the outer surfaces. For storage block temperature T_{block} and ambient temperature T_{amb}, the radiative loss rate is dominated by direct re-radiation through the glass window, proportional to $\left({T_{block}}^4 - {T_{amb}}^4\right)$. Other losses are proportional to the difference between the block temperature

and the surface temperature of the receiver body. Therefore, the total loss rate $q_{out(T)}$ can be modelled by a polynomial of the form:

$$q^*_{out(T)} \approx a\left({T_{block}}^4 - {T_{amb}}^4\right) + b\left(T_{block} - T_{surf}\right) \qquad (4)$$

where a is related to the radiative heat transfer coefficient given by the product of the emissivity (ε) and Stefan-Boltzmann's constant (σ), and b is a combined conduction and convection heat transfer coefficient. This model and the coefficients a, b are believed to be reliable for estimating losses up to the maximum temperature, for example, based on the behaviour of the graphite block where $q_{out(T)}$ data are available from 520 °C. The output from this analysis, plotted as the magnitude of the radiative and linear losses, is shown in Figure 5 for the MGA block during the first solar test.

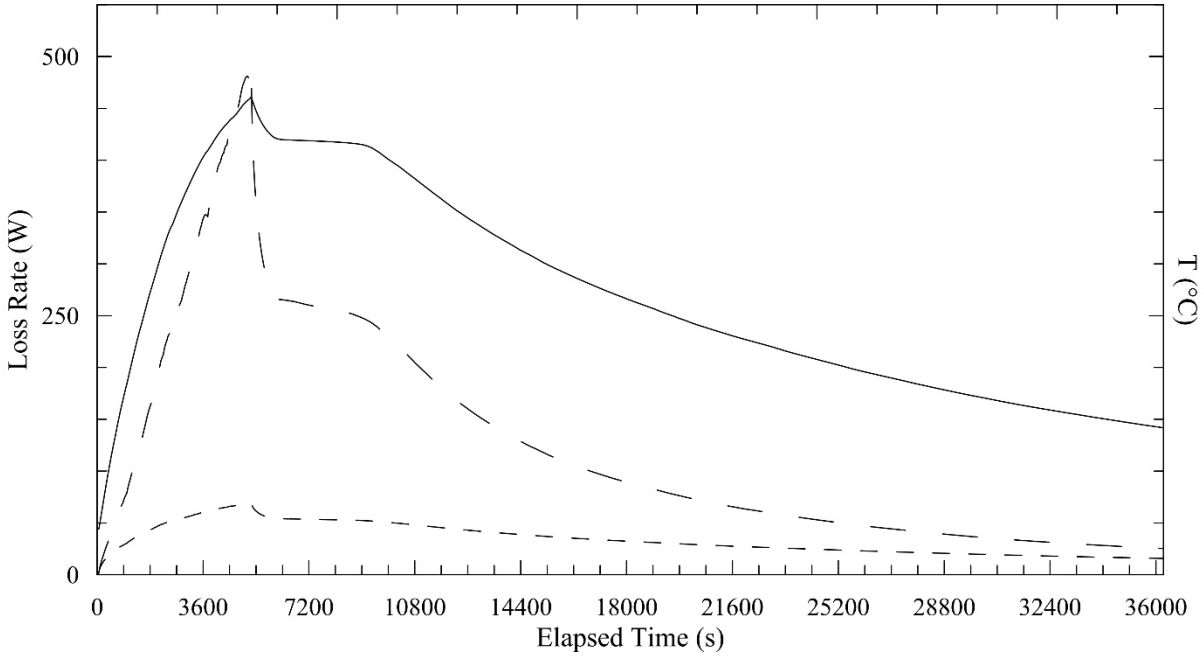

Figure 5 –Mass weighted average block temperature (RH scale), radiative losses (long dashed line, LH scale) and linear losses (short dashed line, LH scale) from C-Zn MGA during the first run.

Re-arranging eq. (1) we obtain eq. (4) which gives an expression for q_{abs}, the power absorbed from the incident radiation prior to re-radiation and conduction into the storage block. In eq. (4), q_{net} is found using experimental data and calculated using eq. (2), and q_{out} is replaced by q^*_{out}, the modelled losses for the entire heating/cooling process.

$$q_{abs} = q_{net} + q^*_{out} \qquad (5)$$

Figure 6 shows the resulting q_{abs} as a function of time as well as the recorded DNI for the full absorption period of the second C-Zn run, although equation (2), and thus eq. (5), is not strictly valid during the phase change, which commences after around 3000 s. It may be seen that the absorbed power q_{abs} tracks the DNI quite well and this is highlighted by the smoothness of the inset plot of q_{abs}/DNI before commencement of the phase change, indicating the reasonableness of the model. For steady state illumination, heat is absorbed at approximately 1.5 kW which equates to an absorbed solar flux of 63 kW/m^2.

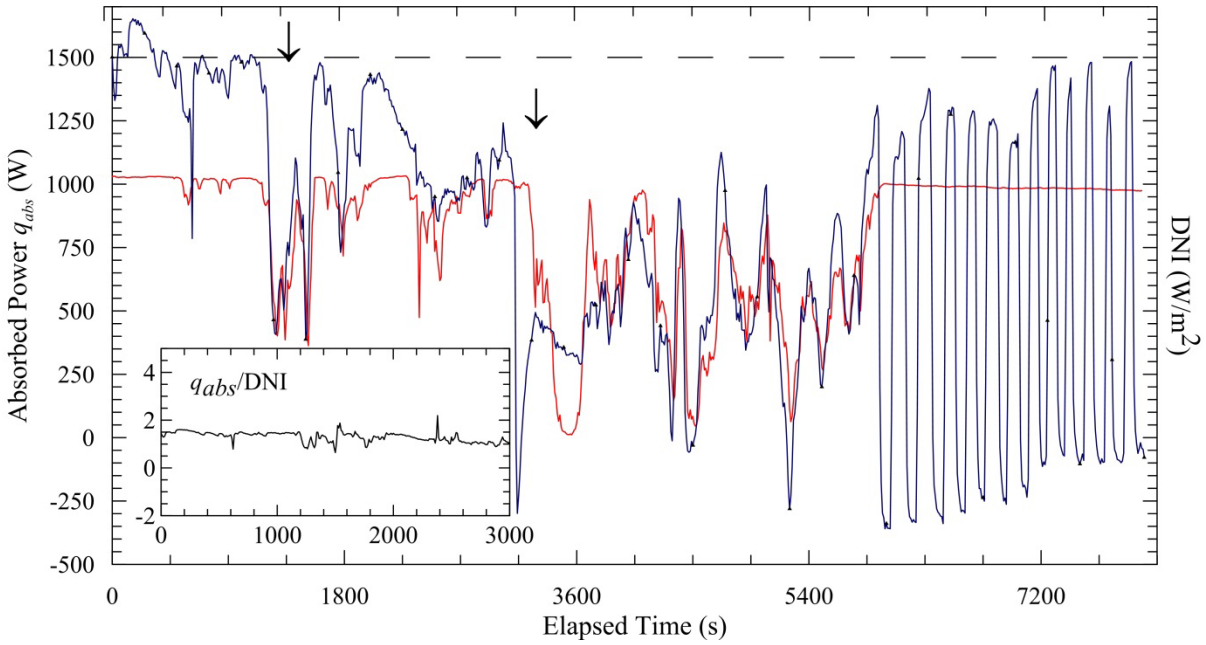

Figure 6 – (Colour online) Total absorbed power, q_{abs} (blue, LH scale) and DNI (red, RH scale) for the second C-Zn run. The inset shows q_{abs}/DNI for heating below commencement of the phase change. A dashed line indicates the estimated steady state absorbed power. The left hand arrow shows an example of excellent correspondence between absorbed power and DNI whereas the right hand arrow shows an example where the phase change has begun to influence the calculation..

Using $q^*_{out(T)}$ as an estimate for $q_{out(T)}$ over the whole temperature range, it is quite simple to convert the temperature data during cooling into the loss rate at each temperature. The quantity of stored energy, Q can be found by integrating between any beginning and end times t_0 and t_1:

$$Q = \int_{t_0}^{t_1} q^*_{out(T)}\, dt \qquad (6)$$

Table 3 summarises the stored energy in these test runs between 370 °C and 470 °C ($T_m \pm 50$) as well as from 200 °C to 470 °C (T_m +50). Comparing the stored energy in Table 3 with the theoretical values in Table 1 indicates that the C-Zn storage block was 80% full during the first run and 99% full during the second run. The majority of the deficit in the first run was because the phase change was only ~65 % complete in that case,

Table 3 – Energy stored during on-sun testing

Material	$Q_{\pm 50}$ (MJ)	$Q_{200-(T_m+50)}$ (MJ)
Graphite	1.02	2.53
C-Zn MGA run#1	1.92	3.45
C-Zn MGA run#2	2.38	3.91

3.3 Thermal Conductivity

One of the characteristic properties of MGA is the theoretically high thermal conductivity of the macroscopically solid block. This allows heat to be rapidly added and removed from the thermal storage

material, resulting in highly dispatchable stored energy. It is possible, through analysis of energy flow and known thermocouple locations, to calculate a coarse value for thermal conductivity (k), using:

$$k = q\left(A\frac{dT}{dx}\right)^{-1} \quad (6)$$

Using the temperature distribution within the blocks and the value for q_{abs} calculated above, we obtain an average *k* value of 151 W/mK for the commercial graphite blocks, and 55 W/mK for the C-Zn MGA at a time when the mass averaged storage block temperature was 300°C. These values generally decrease slightly with increasing temperature. The measurements are in good agreement with the room temperature thermal conductivity quoted for graphite ("Grade PFR Block Specifications", 2018), given as 160W/mK. This gives us some confidence in the conductivity estimate for the MGA.

The measured value of *k* for the MGA is two orders of magnitude above the thermal conductivity for state of the art thermal storage materials (Liu et al., 2012, Xu et al., 2015). While the analysis is rudimentary, it confirms our theoretical expectations from the individual material properties and models of thermal transport in composite materials (Rawson et al., 2013, Rawson et al., 2014, Rawson, 2016) that MGA materials have a much greater capacity to efficiently transport heat when compared with current TES materials.

The measured value of *k* for the C-Zn MGA, is in excellent agreement with the theoretical value of 63 W/mK calculated using the Maxwell-Eucken model by (Rawson, 2016) for the operational range Tm ± 50 °C. The slight reduction in thermal conductivity below the predicted value can be attributed to several factors including some porosity in the storage modules and the effect of small amounts of binder residue, primarily silica phases (Reed et al., 2017). There may also be effects due to contact resistance between thermocouples and the modules or contact resistance between the dispersed phase and the matrix phase however these are thought to be minor given the minimal effect contact resistance has on the inter-block (intra-module) heat transfer.

4. Discussion

The aims of this work were to begin assessment of the feasibility of a greatly simplified thermal storage technology in which the solar receiver, storage and final (only) heat exchanger are all one unit primarily made from an MGA storage block. Given the early stage of MGA development, the areas targeted were; i) an assessment of the scalability of manufacture, ii) the feasibility of assembling large storage blocks from smaller modules, and iii) the response of the material to direct solar irradiation on a solar concentrating dish.

Scale up to 1 L modules and their assembly into storage blocks of arbitrary size was demonstrated in a 4-module block acting as both storage and as a direct solar receiver. At full scale, it is envisioned that storage blocks would be assembled from modules of 0.25 to 0.5 m^3 in size. At the current size of 1 L, surface effects such as die-wall interactions, local damage due to handling and leakage from the few PCM particles that are in direct contact with the surface have already become very minor i.e. a 1 L module is relatively free from these effects. Therefore, it is likely that further scale up will be relatively risk free.

The raw thermocouple data show excellent heat transfer within the storage block both inside modules as shown by data from the central row of thermocouples (Figure 3) and transverse to the storage modules across the inter-module join as shown by the very small temperature variation between different blocks in the 4-module stack due to the large effusivity of MGA materials (Rawson, 2016). MGA storage

modules were stacked into the receiver under only the action of gravity. No special surface preparation was used, nor was any conducting medium used in between the modules. Contact resistance between storage modules within a larger storage block is therefore predicted to have minimal influence on the thermal performance of an MGA storage block assembled from smaller modules.

The results shown in Figure 3 highlight a number of important features. The MGA block was receiving approximately the same solar flux as the graphite; its average heating rate was slightly faster than the graphite until around the melting temperature of the PCM where it slows to below the rate for graphite due to the significant amount of energy being drawn into the melting Zn. The significantly lower thermal diffusivity of the MGA, due to the properties of the Zn, is evident from the increased spread of temperature throughout the storage block. As heating commences, a temperature difference of 110 °C is established between TC1 and TC6 in just 11 minutes. This is maintained over the next 33 minutes, whereupon it falls to 90 °C while the phase change is in full swing before rising to 110 °C again just prior to the end of heating. The temperature profile in this storage block is heavily influenced by the finite depth of the storage block (just 140 mm), the insulated receiver rear wall and lack of any simultaneous heat extraction. In a production MGA block, suitable for CSP thermal storage, the thermal gradient will differ as more heat will be transported deeper into the block.

During cooling below the phase change, the temperature difference between the front and rear thermocouples is very small. For example, heat flow analysis (Figure 5) suggests that during cooling at 350 °C, 200 W is being lost through the front face by radiation with less than 1 °C temperature difference across the storage block. This behaviour suggests that MGA storage blocks are able to undergo rapid temperature equalisation under a range of heat storage and delivery conditions suitable for CSP applications.

The same general conclusions regarding temperature equalisation can be drawn from the second MGA run. During the initial heating of run 2, intermittent cloud cover was present. The ability of the receiver and storage to respond to this is visible in the first 300 s of Figure 6 where there is near perfect correspondence. Once the MGA was above the phase change temperature, no further clouds were encountered. However, to enable complete filling of the storage without exceeding our (somewhat arbitrary) maximum temperature, the dish was oscillated on and off sun towards the end of the heating stage as is visible in Figure 4. The inset to Figure 4 shows how the MGA material is able, within just the 80 mm represented by thermocouples 1-5, to almost completely damp out these oscillations. The combination of the rapid response (e.g. Figure 6, left) and damping, suggest that MGA materials have excellent suitability not only as a thermal storage material, but also as a solar receiver thermal stabilisation backing. This could eradicate both the mechanical effects of thermal shock and the parasitic cost of avoiding salt freezing which have been reported to be of concern in receivers that employ molten salt based cooling (Tyner et al., 1995, Kolb et al., 2002, Ramorakane et al., 2016).

The MGA material used here, C-Zn was shown to be able to absorb a solar flux of approximately 63 W/m^2 from a supplied average flux of 105 W/m^2, i.e. with 60% superficial efficiency. Given that the storage block face is a flat receiver with no solar absorbing coating it represents the worst-case. It is likely that with a deep cavity designed directly into the storage block and the use of a suitable absorbing coating (see for example Karas et al., 2018), the storage block absorption efficiency will increase substantially. MGA materials with considerably higher operating temperature and energy density are available (Reed et al. 2018) and will progressively be incorporated into the testing regime.

Further work is required before macroscopically solid MGA thermal energy storage can be implemented in CSP plants. At a scientific level, the material properties continue to be studied. For

example, experiments to accurately measure the thermal conductivity of C-Zn MGA over a range of temperatures in axes parallel and perpendicular to the pressing direction are under way. These measurements will allow for performance enhancement of receivers/storage/ heat exchanger blocks using MGA materials by orienting the modules to enhance conductivity in certain critical directions. The next stage for this small receiver is to implement active heat extraction during and after thermal charging as well a slight re-design involving:

i) Installing an insulated shutter so that the storage can be protected from radiative losses when charged.
ii) Placing the MGA modules closer to the window and modifying dish utilisation to involve the central mirrors of all petals rather than all mirrors of two petals will reduce the shadowing effect.

A final point to note is that although they were primarily designed for CSP applications, MGA are likely to also be useful for thermal storage in other energy conversion and energy utilisation technologies such as space heating, process heat, waste heat recovery and even fossil fuel power generation.

5. Conclusions

Stable 1 L modules of graphite matrix MGA can be made and are readily assembled into larger thermal storage blocks. MGA storage blocks made this way can absorb direct concentrated solar irradiation at relatively high efficiency for a flat receiver.

Good absorption properties led to rapid heating and this had not saturated at the maximum temperature used (530 °C) with only two petals of mirrors installed. The latent heat contribution to stored energy was visible as a pronounced thermal arrest at 420 °C during cooling in MGA runs 1 and 2 (Figures 4 and 5), the latter lasting for 1.25 hours.

MGA conductivity was estimated at 55 W/mK in reasonable agreement with expectations and was sufficient to allow rapid heat transfer throughout the storage block and rapid equalisation of excursions in the solar flux; either natural (cloud cover) or manmade (on-off sun oscillation). Analysis of heat loss rates showed that direct re-radiation contributed the bulk of the thermal losses close to the phase change temperature.

The use of MGA materials to design new TES systems for CSP and other large scale energy systems involving combination of receiver and thermal storage functions into one unit is shown to be technically feasible under the circumstances of these tests. Further work exploring the incorporation of the primary heat exchanger into the same unit is ongoing.

Acknowledgements

We gratefully acknowledge assistance from the Discipline of Mechanical Engineering workshop at the University of Newcastle and the granting of access to a parabolic solar concentrating dish at the CSIRO Energy Centre, Mayfield West, NSW Australia. Financial support under Australian Research Council Discovery Project grant DP150101257 is also acknowledged.

References

Agyenim, F., Hewitt, N., Eames, P. and Smyth, M. 2010. A review of materials, heat transfer and phase change problem formulation for latent heat thermal energy storage systems (LHTESS). Ren. & Sust. Energy Rev. 14, 615–628.

Alva, G., . Liu, L., Huang, X. and Fang, G., 2017. Thermal energy storage materials and systems for solar energy applications. Ren. & Sust. Energy Rev. 68, 693-706.

Copus, M., Reed, S., Kisi, E.H., Sugo, H.O. & Bradley, J. 2017. Scaling up Miscibility Gap Alloy Thermal Storage Materials. Proceedings World Renewable Energy Congress (WREC XVI), Perth, Australia, 5-9 January 2017.

Dutta, P. 2017. High temperature solar receiver and thermal storage systems. Applied Thermal Engineering, 124, 624–632.

Fukahori, R., Nomura, T., Zhu, C., Sheng, N., Okinaka, N., & Akiyama, T. 2016. Macro-encapsulation of metallic phase change material using cylindrical-type ceramic containers for high-temperature thermal energy storage. Applied Energy, 170, 324–328.

Gomez, J. 2011. High-Temperature Phase Change Materials (PCM) Candidates for Thermal Energy Storage (TES) Applications. NREL Milestone Report NREL/TP-5500-51446.

Gonzalez-Gomez, P.A., Gomez-Hernandez, J. and Briongos, D.S. 2017. Thermo-economic optimization of molten salt steam generators. Energy Conversion and Management 146, 228-243.

González-Roubaud, E., Pérez-Osorio, D., & Prieto, C. 2017. Review of commercial thermal energy storage in concentrated solar power plants: Steam vs. molten salts. Renewable and Sustainable Energy Reviews, 80, 133–148.

Herrmann, U., Kelly, B. and Price, P. 2004. Two-tank molten salt storage for parabolic trough solar power plants. Energy 29, 883-893.

IRENA. 2013. Concentrating Solar Power - Technology Brief. Retrieved from https://www.irena.org/DocumentDownloads/Publications/IRENA-ETSAP Tech Brief E10 Concentrating Solar Power.pdf

Karas, D.E., Byun, J., Moon, J. and Jose, C. 2018. Copper-oxide spinel absorber coatings for high-temperature concentrated solar power systems. Solar energy materials and solar cells 182, 321-330.

Kenisarin, M.M., High-temperature phase change materials for thermal energy storage. Renewable and Sustainable Energy Reviews 2010; 14: 955-970.

Khan, Z., Khan, Z. and Dhafoor, A. 2016. A review of performance enhancement of PCM based latent heat storage system within the context of materials, thermal stability and compatibility. Energy Conversion and Management 115, 132-158.

Kolb, G., Pacheco, J. E., & Showalter, S. 2002. Final Test and Evaluation Results from the Solar

Two Project. http://doi.org/10.2172/793226

Kuravi, S., Trahan, J., Goswami, D.Y., Rahman, M.M. and Stefanakos, E.K. 2013. Thermal energy storage technologies and systems for concentrating solar power. Progress in Energy and Combustion Science 39, 285-319.

Laing, D., Bahl, C., Bauer, T., Fiss, M., Breidenbach, N. & Hempel, M. 2012. High-temperature solid media thermal energy storage for solar thermal plants. Proceedings of the IEEE 100(2), 516-524.

Liu, M., Saman, W. and Bruno, F. 2012. Review on storage materials and thermal performance enhancement techniques for high temperature phase change thermal storage systems, Ren. & Sust. Energy Rev. 16, 2118– 2132.

Parabolic Trough Projects | Concentrating Solar Power| NREL. Retrieved July 4, 2018, from https://www.nrel.gov/csp/solarpaces/parabolic_trough.cfm

Pelay, U., Luo, L., Fan, Y., Stitou, D. and Rood, M. 2017. Thermal energy storage systems for concentrated solar power plants. Ren. & Sust. Energy Rev. 79, 82-100.

Power Tower Projects | Concentrating Solar Power |NREL. Retrieved July 4, 2018, from https://www.nrel.gov/csp/solarpaces/power_tower.cfm

Ramorakane, R. J., Dinter, F., Eng, P., Electro-Mechanical, E., & Eng, M. 2016. Evaluation of parasitic consumption for a CSP plant. AIP Conference Proceedings, 0700271(10). http://doi.org/10.1063/1.4949174

Rathod, M.K. & Bannerjee, J. 2013. Thermal stability of phase change materials used in latent heat energy storage systems: A review. Renewable and Sustainable Energy Reviews 18, 246-258.

Rawson, A. 2013. Characterising Thermal Properties of Miscibility Gap Alloys for Thermal Storage Applications. In Proceedings of the 52nd Annual Conference. Melbourne: Australian Solar Council. Retrieved from http://solar.org.au/papers/14papers/98_final.pdf

Rawson, A. J. 2016. PhD Thesis, The University Of Newcastle. Modelling and application of advanced thermal storage materials.

Rawson, A., Kisi, E., Sugo, H., & Fiedler, T. 2014. Effective conductivity of Cu–Fe and Sn–Al miscibility gap alloys. International Journal of Heat and Mass Transfer, 77, 395–405. http://doi.org/10.1016/j.ijheatmasstransfer.2014.05.024

Reed, S., Sugo, H. & Kisi, E.H. 2017. New highly thermally conductive thermal storage media, Proceedings World Renewable Energy Congress (WREC XVI), Perth, Australia, 5-9 January 2017.

Reed, S., Sugo, H. and Kisi, E. 2018. High Temperature Thermal Storage Materials with High Energy Density and Conductivity. Solar Energy, 163, 307-314.

Sarvghad, M., Maher, S.D., Collard, D., Tassan, M., Will, G. and Steinberg, T.A. 2018. Materials compatibility for the next generation of concentrated solar power plants. Energy Storage Materials,

14, 179-198.

Sugo, H.O., Kisi, E.H. and Cuskelly, D.T. 2013. Miscibility gap alloys with inverse microstructures and high thermal conductivity for high energy density thermal storage applications. App. Therm, Eng. 51, 1345-1350.

Tian, Y. and Zhao, C.Y. , A review of solar collectors and thermal energy storage in solar thermal applications. Applied Energy 2013; 104: 538-553.

Tyner, C. E., Sutherland, J. P., & Gould, W. R. 1995. Solar Two: A Molten Salt Power Tower Demonstration*. Retrieved from

http://large.stanford.edu/publications/coal/references/docs/1605696.pdf

Xu, B., Li, P., & Chan, C. 2015. Application of phase change materials for thermal energy storage in concentrated solar thermal power plants: A review to recent developments. Applied Energy, 160, 286–307. http://doi.org/10.1016/J.APENERGY.2015.09.016